Cellular network formation of hydrophobic alkanethiol capped gold nanoparticles on mica surface mediated by water islands

Neena S. John,[1,a)] Gargi Raina,[2] Ashutosh Sharma,[3,b)] and Giridhar U. Kulkarni[1,c)]
[1]*Chemistry and Physics of Materials Unit, DST Unit on Nanoscience and CSIR Centre of Excellence in Chemistry, Jawaharlal Nehru Centre for Advanced Scientific Research, Jakkur P.O., Bangalore 560064, India*
[2]*School of Electrical Sciences, Vellore Institute of Technology, Vellore 632014, India*
[3]*Department of Chemical Engineering, Indian Institute of Technology, Kanpur 208016, India*

(Received 25 June 2010; accepted 11 August 2010; published online 7 September 2010)

Dendritic and cellular networks of nanoparticles are known to form commonly either by random diffusion-limited aggregation or by solvent evaporation dynamics. Using alkanethiol capped gold nanoparticles deposited on mica imaged under ambient and controlled water vapor conditions by atomic force microscope and *in situ* scanning electron microscope, respectively, we show a third mechanism in action. The cellular network consisting of open and closed polygons is formed by the nucleation and lateral growth of adsorbed water islands, the contact lines of which push the randomly distributed hydrophobic nanoparticles along the growth directions, eventually leading to the polygonal structure formation as the boundaries of the growing islands meet. Such nanoparticle displacement has been possible due to the weakly adhering nature of the hydrophilic substrate, mica. These results demonstrate an important but hitherto neglected effect of adsorbed water in the structure formation on hydrophilic substrates and provide a facile tool for the fabrication of nanoparticle networks without specific particle or substrate modifications and without a tight control on particle deposition conditions during the solvent evaporation. © *2010 American Institute of Physics*. [doi:10.1063/1.3484941]

I. INTRODUCTION

Stability, aggregation, and pattern formation in nanoparticles on surfaces are of interest in both scientific and technological research. Particles are usually coated with passivating molecules to prevent against surface modification and agglomeration upon removal of the dispersing medium in the ambient. In the recent years, the use of self-assembling molecules to cap nanoparticles enabled direct assembly of particles as against simple aggregation. For instance, monodispersed metal[1–3] and semiconductor[4] nanocrystals have been coated with a variety of molecules, such as alkanethiols, alkylamines, and fatty acids, and biomolecules, such as DNA, etc.,[5] and programed assemblies have been obtained in one, two, and three dimensions. By coating with polymeric ligands, giant clusters of nanocrystals of definite nuclearity have also been obtained.[6] The research in this area has also been motivated by the fascinating electrical, optical, and magnetic properties exhibited by nanocrystal assemblies constituting metals, semiconductors, or binary alloys that find applications in nanodevices.[7–9] The simplest method of obtaining mesoscalar arrays is by the spontaneous aggregation of particles either reversibly or irreversibly to form cellular networks or dendrimeric assemblies. Such irreversible kinetic aggregation of colloids has been observed in soot particles, citrate stabilized gold nanocrystals in aqueous medium coagulated by adding pyridine, and also on surfaces when the dispersion medium is allowed to evaporate, leaving behind the nanoparticles. The spontaneous aggregation of nanoparticles on surfaces when the solvent is allowed to evaporate has been utilized to get various nanostructures in the form of rings and other shapes.[10] The mechanism in the above case was explained by the Marangoni convection, as also is the case of pattern formation by an evaporating solvent drop on a soluble polymer layer.[11] Moriarty *et al.*[12] reported the formation of cellular networks of Au nanocrystals capped with alkanethiols when spin coated with a toluene solution of the nanocrystals on a silicon surface. Extensive experiments involving the dewetting of thin films and simulations have provided important insights into the mechanism underlying the formation of such networks mediated by the formation, growth, and coalescence of holes in the solvent layer carrying the particles.[13–19] Fractal and tessellation analyses of the patterns and nanoparticle distribution have also aided the understanding of growth mechanisms.[12,20–24] For describing the scale invariance of the geometrical arrangement of the particles in a cluster, fractal dimension is a frequently used parameter in the theoretical as well as the experimental investigations. Experimentally, direct particle size analyses from transmission electron microscope (TEM) and atomic force microscope (AFM)/scanning tunneling microscope images and indirect analyses from optical as well as neutron scattering measurements are the usual methods for determining the fractal dimension.

While earlier studies have focused on the role of solvent evaporation in obtaining different nanoparticle assemblies on surfaces, we show here that the nucleation and growth of

[a)]Electronic mail: jsneena@gmail.com.
[b)]Electronic mail: ashutos@iitk.ac.in.
[c)]Electronic mail: kulkarni@jncasr.ac.in.

adsorbed water microdomains on the substrate play an important role in the formation of hydrophobic nanoparticle networks on hydrophilic substrates. Although it is known that water vapor adsorbed on hydrophilic mica shows fascinating dynamics and order,[25] its role in pattern formation of nanoparticles has not been appreciated. In order to examine the role of adsorbed/condensed water islands in the formation of network, we report *in situ* experiments on the aggregation of thiol capped Au nanoparticles on mica with the introduction of water vapor in the vacuum chamber of a field-emission scanning electron microscope (SEM). We also compare these results to a more common, but less controlled, experimental protocol where the particle aggregation is induced under the ambient conditions and observed by AFM. Under the ambient conditions, we track the particle aggregative patterns at various time intervals and could thus analyze different stages of pattern formation. We show that relatively big isolated clusters of nanoparticles deposited by solvent evaporation are gradually transformed first to branched networks and then to a closed polygonal network as the time progresses. Further, by examining the size dependent mobilities of nanoparticle clusters, we suggest that the network structure is not caused by a simple random diffusion-limited growth, but that the presence of water plays an active role in the network formation. Tesellation and fractal analyses have been performed on the network structures. Understanding the mechanisms involved in the condensation and growth of nanoparticle aggregates should provide more control and flexibility in the organization of nanoparticles for specific applications.

II. EXPERIMENTAL METHODS

Au nanoparticles capped with dodecanethiol were prepared following the method of Brust *et al.*[26] Briefly, 1 ml (25 mM) $HAuCl_4$ in 10 ml water was phase transferred to the toluene by vigorously shaking it with 220 mg of tetraoctylammonium bromide in toluene layer, followed by the addition of 82 μl of dodecanethiol and reduction with 10 ml of 0.2*M* sodium borohydride in water. The nanocrystals were purified by repeated precipitation with excess methanol and redispersed in toluene for further use. Transmission electron microscopic measurements were carried out with a JEOL-3010 TEM operating at 300 kV. Samples for TEM were prepared by evaporating a drop of toluene solution on a holey carbon copper grid.

AFM characterization was performed using CP-II AFM setup (Veeco Metrology, Santa Barbara). The imaging was done in noncontact ac mode using a Si cantilever with a resonant frequency of 270 Hz under ambient conditions (relative humidity of ~40%). 10 μl of the dilute dispersion (ten times the dilution of the original solution) of the particles in toluene was drop cast on a mica surface for AFM studies. The mica surface was freshly cleaved before the deposition of particles so that the surface is free of any water film or foreign particles and thereafter stored in ambient for spontaneous evaporation of the solvent.

High resolution scanning electron microscopy was preformed using a field-emission SEM (Nova NanoSEM600, FEI, The Netherlands) operating at 0.5–1 kV beam voltage. In the high vacuum mode, through-lens detector was employed, while in low vacuum mode, a helix detector was employed to obtain high resolution images. In order to study the influence of water film on the organization of particles on mica, water vapor (0.4–0.9 Torr) was introduced into the SEM chamber for several minutes, in the "environmental low vacuum mode." Images were captured while the vapor was on or off.

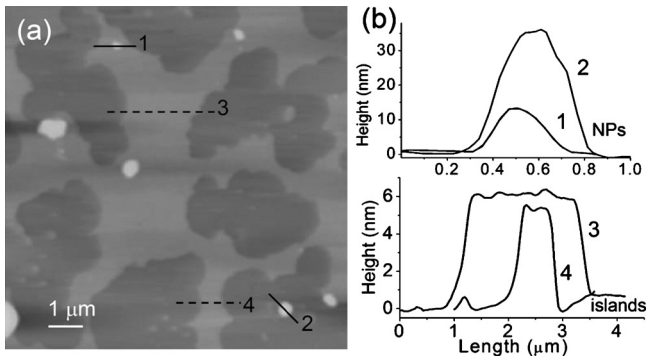

FIG. 1. (a) AFM image of water islands and Au NPs on mica. The brighter spots correspond to nanoparticles (NPs). (b) Section analysis of NPs and water islands.

III. RESULTS

With the mica surface being hydrophilic, it hosts water in the form of islands when exposed to ambient conditions, as described in several studies.[27–29] Thus, the nanoparticles on the mica surface is actually an intricate three-phase system of substrate-adsorbed water islands-air with nanoparticles where the aggregation of nanoparticles produces another microphase. Here, the organization of nanoparticles should be determined not only by their interactions with the substrate but also by the morphology and dynamics of water islands. Further, interactions with the adsorbed water also depend on the particle surface hydrophobicity, which could be modified by a hydrophobic ligand. In this context, water insoluble hydrophobic nanoparticles showing little adhesion to hydrophilic mica are preferred because their aggregation could be easily directed by the three-phase contact lines of water islands that could push particles without engulfing them.

We first describe the results of nanoparticle pattern formation under ambient conditions over a long time period after their deposition on the mica by drop casting from a relatively rapidly evaporating solvent, toluene. This preliminary experiment is a guide to show the robustness of aggregation phenomenon even under the common laboratory conditions. The structures were imaged by an AFM under ambient conditions. Figure 1 shows one such area of a mica substrate deposited with thiol capped Au nanoparticles. Interestingly, during AFM imaging, relatively large water islands of differing widths (1–3 μm), with a thickness of ~5–6 nm, are observed on the mica surface (see Fig. 1) interspersed with nanoparticles. In fact, if a freshly cleaved mica surface is scanned in AFM, one can also observe the formation of these water islands that may also be aided by

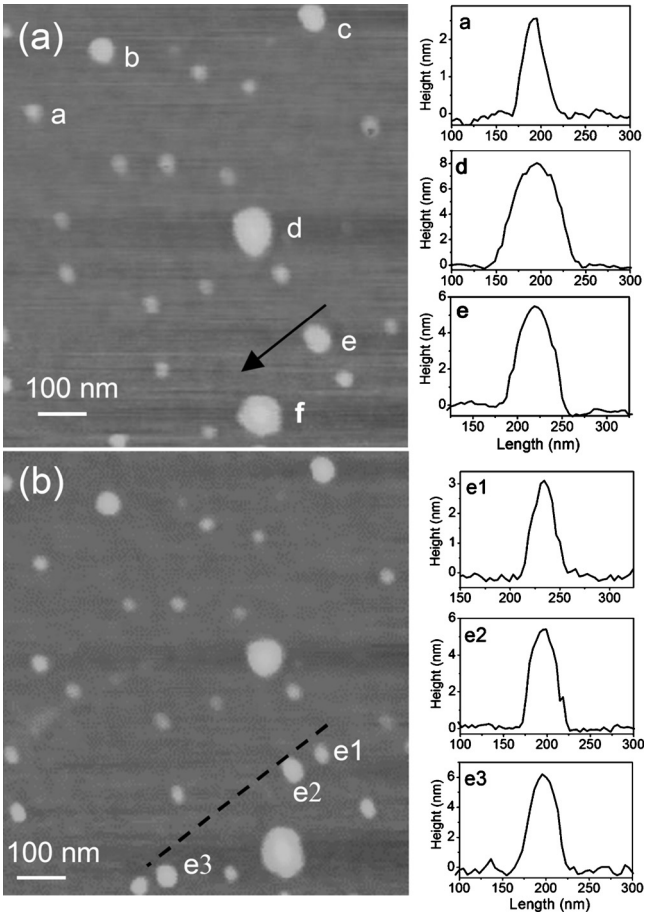

FIG. 2. (a) AFM topography of dodecanethiol capped Au nanoparticles as deposited on a freshly cleaved mica surface. The particle marked a represents an individual particle whose z profile is shown along side, with $z=2.8$ nm. The particles marked b–f are bigger aggregates, the z profile of d and e are shown, with $z=8$ and 5.2 nm. Aggregate e with a black arrow shows the direction in which it was laterally pushed using the nanomanipulation utility. (b) AFM image showing the status after nanomanipulation. Aggregate e got split into e1, e2, and e3 (lying on dotted line) and their corresponding height profiles are given.

the condensation of water from nanometric AFM tip to the surface by capillary action.[28] Section analysis of the nanoparticles on the mica surface gives the height variation in the range of tens of nanometers, while the diameters are in the range of hundreds of nanometers, indicating that these are nearly two-dimensional (2D) aggregates of nanoparticles [Fig. 1(b)]. The mean individual particle size estimated from TEM analysis is ~3 nm.[30] Hence, solvent evaporation upon deposition on mica leads to the aggregated nanoparticle clusters. From the AFM height profile analysis, hundreds of nanoparticles are present in an aggregated cluster.

The formation of nanoparticle aggregates on the surface following solvent evaporation is a commonly observed phenomenon and may arise due to the solvent dewetting mechanisms.[31] However, the particle aggregation observed in this study may have a contribution from water islands as well.

The mobile nature of Au nanoparticles over the mica surface is confirmed from the AFM images captured within a 15 min interval, as shown in Fig. 2. The water islands seen in Fig. 1 formed via condensation from the AFM tip must have evaporated in the course of time, leaving a molecularly thin water layer on the mica surface[28] that is not visible in the given z-range of the AFM image. Figure 2(a) shows an area selected for nanomanipulation comprising of comparatively smaller aggregates widely separated from each other by an average distance of 200 nm. Although the height profiles of very small aggregates correspond to the diameter of an individual particle (see the height profile of feature "a"), the lateral dimensions (28–45 nm) are larger than the vertical height. The figure also shows some bigger features where diameters are several times higher than the individual nanoparticles. Thus, the diameters of features b–e are in the range of 50–90 nm, with heights in the range of 5–8 nm [see Fig. 2(a)]. The height profiles of bigger aggregates, "d" and "e," are also shown in Fig. 2(a). The number of nanoparticles within an aggregate also scales with the aggregate size.[30] However, aggregates with diameters in the range of 28–45 nm show a dispersion in the number of particles they contain, which might be arising from the original particle size distribution. These aggregates contain only a monolayer of particles, while larger diameter aggregates contain almost a bilayer or multilayers of nanoparticles. The formation of spherical aggregates randomly distributed shows that the directive nature of the thiols to form an assembly has vanished in this case.

We tried to push the aggregate with the AFM tip [marked as e in Fig. 2(a)] in the lateral direction [indicated by the arrow in Fig. 2(a)]. In Fig. 2(b), we show the result of nanomanipulation, which reveals that the parent aggregate e split into two other features: e2 and e3. We observe that the parent aggregate has retained some amount of material [marked as e1 in Fig. 2(b)]. All the three aggregates, e1, e2, and e3, seem to lie in the direction along which nanomanipulation was carried out (see the dotted line in the figure). A simple calculation gives the volume of daughter aggregates as ~12 304 nm^3, which is slightly larger than the parent aggregate, ~11 608 nm^3. This may be because of the addition of some nanocrystals in the path of manipulation, from either the surface or the tip itself, or the breaking cluster may have become slightly more porous.

We have calculated the displacement of the aggregates in the image frames given in Figs. 2(a) and 2(b), captured in an interval of a few minutes, to examine their mobile nature. Almost 30 aggregates from two successively captured AFM images have been analyzed to arrive at the plot of mobility of aggregates. In Fig. 3, the vectorial (x,y) displacements of aggregates of various sizes are presented. The volumes were calculated from the measured diameter and height values assuming a spherical cap shape. Interestingly, there is no trend in the displacement with the cluster size. In particular, a large dispersion in the displacement is observed for aggregates of smaller sizes. Medium sized aggregates are not found to move a whole lot, while a relatively large aggregate seems to have been displaced considerably.

When the sample was kept undisturbed in a dust free environment but still in ambient for several weeks, we observed a progressive aggregation of nanoparticles. The AFM images shown in Fig. 4 are a typical illustration of the aggregation process in its different stages. After 3 weeks of

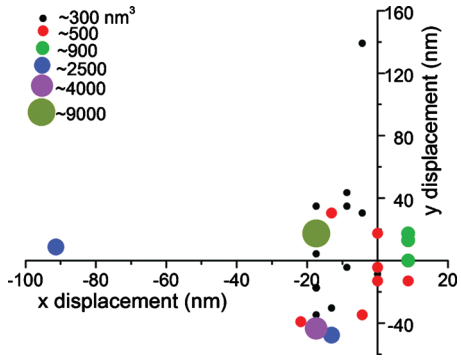

FIG. 3. A plot of the vectorial (x,y) displacement of the aggregates with various volumes. The displacement was calculated from the Cartesian coordinates of the aggregates with respect to the aggregate "f" [shown in Fig. 2(a)], taken as the origin. Aggregate f, being a larger aggregate, is assumed to be immobile and aggregate e is not considered. The size of the circular symbols is depicted to increase with volume.

exposure to ambient, particle aggregation leading to branched chain structures is seen by AFM imaging [Fig. 4(a)]. The formation of a cellular network nanostructure is clearly observed. Intense bright spots in the image correspond to dense aggregates. Figure 4(b) gives the AFM image of the sample captured after a few more days of exposure to ambient, showing a fully developed network structure. The cell-to-cell distance is in the range of 1–1.6 μm. A cross-

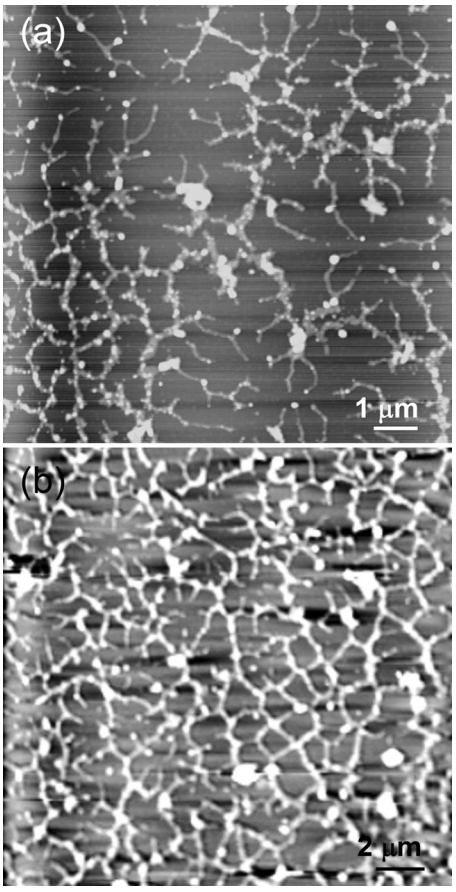

FIG. 4. AFM topography of the different stages of the growth of thiol capped Au NPs on the mica surface. (a) The intermediate stage before the closing of the branches to form polygonal network. (b) The cellular network formed from the nanoparticles.

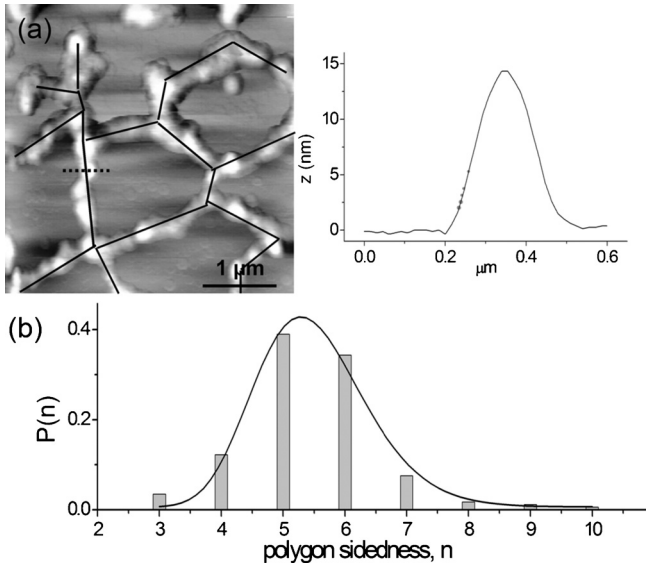

FIG. 5. (a) The tessellation analysis of the cellular network. The black lines drawn over the network show the way in which the polygon distribution was obtained. The z profile taken along a line (dotted line) through the side of a polygon is also given. (b) A histogram showing the distribution of polygon sidedness in the cellular network. A log normal fit to the distribution gives the mean polygon sidedness as 5.4.

sectional profile taken across the polygon side [Fig. 5(a)] shows the height to be 15 nm, indicating that the brighter spots consist of multilayers of nanoparticles. A height variation of 5–25 nm is observed for less bright spots to intense bright spots corresponding to a monolayer and multilayers of Au nanoparticles, respectively. The larger aggregates seen in Fig. 4(a) become relatively immobile, but the individual nanoparticles continue to diffuse to complete the polygonal sides, leading to the closed network structure in Fig. 4(b). Gold nanoparticles coated with dodecanethiol are hydrophobic and thus should readily diffuse on the hydrophilic mica surface, which may also be covered by a monolayer or a partial monolayer of water. This is also evident from the ease of displacing the clusters in our nanomanipulation experiments where the particles exhibited negligible adhesion to the substrate.

The nature of the cellular networks formed by nanoparticles has been examined in detail. A statistical analysis of the tessellation was performed.[32] Figure 5(a) is a representation of how the polygons have been drawn over the network for the analysis. Several large area AFM images were considered for this purpose. The tessellation analysis gives a histogram of polygon sidedness distribution with a mean value of 5.4, as shown in Fig. 5(b). The value is slightly less than 6, which is expected for a stable network and might be an indication of the network coarsening.[32]

In order to examine the role of water islands in the formation of network, *in situ* experiments were performed in the vacuum chamber of a field-emission SEM with gradual introduction of water vapor. Thiol capped Au nanoparticles were deposited on a freshly cleaved mica surface, which was then immediately introduced into the vacuum chamber. The SEM image in Fig. 6(a) shows the presence of already aggregated particles left by the vaporization of toluene. Subse-

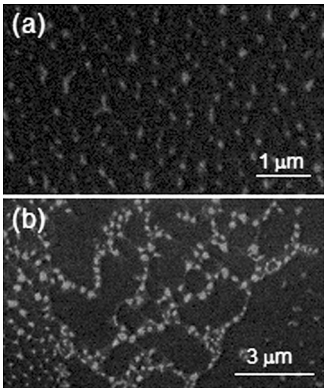

FIG. 6. FESEM images of Au NP network formation on mica monitored *in situ* in a vacuum chamber while introducing water vapor. (a) Thiol capped Au NPs just after the deposition on mica and before the introduction of water vapor. (b) After a few minutes of introducing water vapor in the chamber.

quently, water vapor was introduced into the chamber and within a few minutes, we observed signatures of the formation of network, as can be seen in Fig. 6(b). This indicates that water islands play a major role in the network formation as discussed later. The particle aggregates did not assemble until the water vapor was introduced.

We have also examined the fractal dimension of the network using the lake-filling model,[33] available with the fractal analysis software utility of CP-II AFM. The perimeter length, L, and area, A, of the fractal aggregate are related by $L(\delta) = \alpha D' A^{D'/2}$, where α is a constant, δ is the yardstick length (length of a pixel), and D' is the fractal dimension. With a moderate z threshold of 11.2 nm and neglecting lakes with area smaller than $30\delta^2$, we could obtain isolated lakes, as

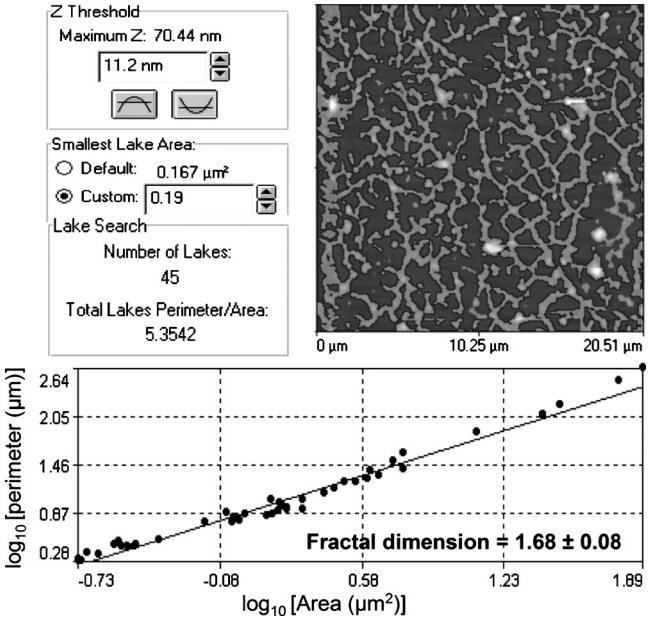

FIG. 7. Fractal analysis of the cellular network performed using the utility software of CP-II, based on a lake-filling algorithm. The image shows the filling of lakes depending on the *z* and area threshold one chooses. A log-log plot of perimeter of the lakes having non-neighbor lakes against the area of the lakes gives a straight line. The fractal dimension determined from the slope is 1.68.

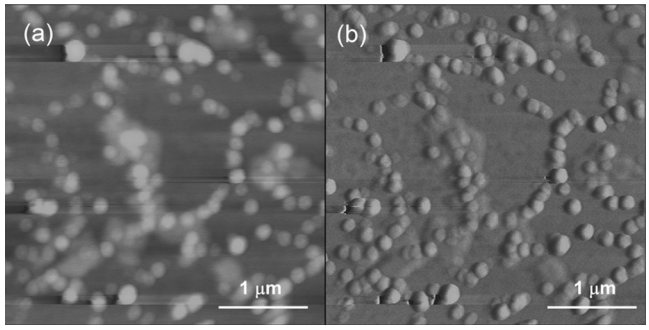

FIG. 8. Tapping mode AFM images of Au NP network on mica after heating. (a) Topography. (b) Phase image.

shown in Fig. 7. A plot of log L versus log A showed a straight-line behavior with a slope of 0.84. The fractal dimension in 2D calculated as 2× slope is 1.68. Consistent values (error bar is ±0.08) were obtained for images captured from other regions of the sample.

The stability of the cellular network of nanoparticles on mica was examined by heating the substrate to 230 °C for 1 h. Subsequent AFM imaging showed that the network structure is only partially altered, but not completely destroyed. However, the particles surprisingly now appear to be rather uniform in size (8 nm in height), as shown in Fig. 8. Evidently, the retraction of water islands on heating does not exert enough pull to at least the weakly adhering bottom layer of particles to destroy the polygonal outlines. It is expected that the random mobility of the particles, especially at this elevated temperature, can affect the polygonal shapes.

IV. DISCUSSION

Au nanoparticle networks obtained on the mica surface are morphologically similar to the observations on silicon surfaces.[12,24] However, the network obtained here under ambient conditions slowly evolves over a long period of time, and hence intermediate stages of aggregation could be captured. In addition, the network is composed of multilayers of particles. Several mechanisms have been suggested in literature for explaining the aggregation of nanocrystals formed under different experimental conditions. In some cases, the aggregation may be because of the random Brownian movement, the collisions and capture of the particles resulting in aggregation. However, in our case, we see a large dispersion in the movement of aggregates with similar size in a time interval of a few minutes (see Fig. 3) without any clear size dependence. Also, *in situ* SEM studies show that a similar pattern of aggregation and network formation can take place in a highly humid atmosphere within minutes (see Fig. 6)—thus ruling out random diffusion-limited growth as a mechanism. Initial solvent evaporation and dewetting induced particle aggregation has also been proposed in the case of a thin spin coated layer of Au particles on Si substrate.[18,19] The particle network formation in this case occurs by the formation of growing holes in the evaporating thin layer. The retracting three-phase contact line and the liquid carries particles with it. Eventually, the merging of holes leads to a cellular network of particles. In this process, the network structures form immediately during the solvent deposition

process itself. In the case of controlled pattern formation demonstrated by directing the solvent dewetting mediated by solvent meniscus or substrate modifications,[14,15] the type of nanoparticle assembly formed depends on the local evaporation time, contact line dynamics, and particle adhesion to the substrate vis-à-vis to the expanding contact line. Both the theory and experimental aspects of pattern formation during solvent evaporation are now fairly well understood,[13] where the basic physics is already captured by the formation, growth, and coalescence of holes in unstable thin films.

However, in the system studied here, the solvent evaporation initially produces randomly distributed nanoparticle clusters, rather than the final cellular network, which results slowly under relatively dry ambient conditions or very rapidly by nucleation and growth of induced water islands. This clearly argues for an active role of adsorbed water in the evolution of hydrophobic particle network on the mica surface. With the mica being hydrophilic, "icelike" water islands form on the surface [Fig. 1(a)]. There are various reports on adsorbed water and the structure and dynamics of its thin films.[25,27,28] Water adsorbed on mica forms icelike water islands when exposed to a humid environment. In a detailed study, Salmeron and co-workers[27,28] identified two phases of water structures on mica—phase II, being the ice islands with boundaries resembling polygonal sides in a relative humidity of 20%–40%. With the relative humidity in our case being 40%, these islands with polygonal boundaries form on mica either upon exposure to ambient water or in controlled vapor atmosphere or facilitated by AFM scanning. We thus propose a nucleation/condensation and subsequent liquid island growth as the mechanism of particle displacement and the network formation of thiol capped Au nanoparticles on mica. Initially, the particles drop cast on the fresh mica surface form randomly distributed larger aggregates due to the slow evaporation and dewetting of toluene. AFM and SEM images show the presence of isolated aggregates just after deposition [Figs. 2(a) and 6(a)]. The network formation is induced in a second step by exposing to water vapor and thus by nucleation and growth of water islands, the boundaries (contact lines) of which push particles along the growth directions and loosen the large aggregates, thus eventually forming a network structure as the boundaries of growing islands meet each other [Figs. 4 and 6(b)]. The resultant network structures closely resemble the polygonal boundaries of the water islands that support the suggested mechanism. Recently, there has been a report of the fractal aggregates formed by citrate stabilized Au nanoparticles on the mica surface, but mediated by the dissolution of a preadsorbed polyelectrolyte/surfactant film following the wetting of mica.[34] Here, we show that such a network can also be obtained on mica by the spontaneous aggregation and redistribution engendered by the growth of adsorbed water islands. Interestingly, this mechanism has both similarities and contrasts with the mechanism of network formation by the nucleation and growth of holes in a particle laden evaporating solvent film. In our case, it is the three-phase contact line of nucleated and growing water islands that pushes (rather than pulls) the particles to complete the polygonal network formation. The advancing water island boundary now serves a similar role as in the nanomanipulation with AFM discussed earlier. Clearly, the selection of one of these two competing mechanisms should depend on the method of initial particle deposition and the effectiveness of the three-phase line to either push or pull a particle cluster along. The latter depends on the adhesion of a particle to the substrate vis-à-vis to the advancing or retracting contact line and particle solubility in the carrier liquid medium. Thus, one of the implications of this work is that different methods of initial particle deposition and different surface properties of the particle and substrate, e.g., hydrophobicity and adhesion, may produce different outcomes. In any case, in those systems where the initial solvent evaporative step fails to produce a network structure, the long time equilibrium limit under humid conditions can transform them to a cellular network.

Our estimation of the fractal dimension of network as 1.68 ± 0.08 is close to the value obtained for the diffusion-limited aggregation process. There are especially two classes of aggregation reported for gold colloid in aqueous medium—diffusion-limited aggregation (DLA) with fractal dimension (D) = 1.75 and reaction-limited aggregation (RLA) with a D = 2.05. In DLA, the rapid aggregation of nanoparticles is controlled by the diffusion of the particles, while in RLA, a slower rate of aggregation is controlled by the reaction conditions rather than diffusion. From a controlled study of gold colloid coagulation by pyridine addition, Weitz *et al.*[35] expressed the limits for the irreversible kinetic aggregation of gold colloids as $1.75 \leq D \leq 2.05$. The growing water islands forces the particle aggregates to diffuse along the boundaries. When the repulsive interactions between them are overcome, further aggregation results in fractal networks.

V. CONCLUSIONS

We have investigated the cellular network formation of thiol capped gold nanocrystals on the mica surface by AFM and by SEM, both in ambient conditions and by deliberate introduction of water vapor. Aggregates of nanocrystals initially form on the mica surface during solvent dewetting when the nanocrystal dispersion is drop cast on the surface. These large aggregates evolve into a complete cellular network with time under ambient conditions. In contrast to the cellular network reported in literature that form either because of solvent dewetting or spinodal decomposition, the network formation in our case is engendered by the growth of adsorbed water islands. A tessellation analysis has shown that the network evolves continuously. We attribute the network formation to the nucleation and growth of water islands; the boundaries of which can readily push the hydrophobic thiol capped nanocrystal aggregates along the growth directions. The final meeting of the contact lines produces a closed network. The role of water islands in network formation is supported by *in situ* SEM studies wherein the formation of network is observed within a few minutes after the introduction of water vapor into the chamber. The nanocrystal network is found to be partially stable to heat. The fractal dimension of the network has been calculated by applying lake-filling model to AFM data and the value is 1.68, similar to a diffusion-limited-like aggregation process.

ACKNOWLEDGMENTS

The authors thank Veeco India Nano Laboratory for providing the AFM facility. This work was supported by DST grants to G.U.K. and A.S. (DST-IRHPA). N. R. Selvi is acknowledged for the technical help with SEM.

[1] M. Brust, M. Walker, D. Bethell, D. J. Schiffrin, and R. Whyman, Chem. Commun. (Cambridge) **1994**, 801.
[2] S. Sun and C. B. Murray, J. Appl. Phys. **85**, 4325 (1999).
[3] L. O. Brown and J. E. Hutchison, J. Phys. Chem. B **105**, 8911 (2001).
[4] C. B. Murray, C. R. Kagan, and M. G. Bawendi, Science **270**, 1335 (1995).
[5] A. P. Alivisatos, K. P. Johnsson, X. Peng, T. E. Wilson, C. J. Loweth, M. P. Burchez, Jr., and P. G. Schultz, Nature (London) **382**, 609 (1996).
[6] P. J. Thomas, G. U. Kulkarni, and C. N. R. Rao, J. Phys. Chem. B **105**, 2515 (2001).
[7] C. T. Black, C. B. Murray, R. L. Sandstrom, and S. Sun, Science **290**, 1131 (2000).
[8] C. N. R. Rao, P. J. Thomas, and G. U. Kulkarni, *Nanocrystals: Synthesis, Properties and Applications*, Springer Series in Materials Science Vol. 95 (Springer-Verlag, Berlin, 2007).
[9] R. Muszynski, B. Seger, and P. V. Kamat, J. Phys. Chem. C **112**, 5263 (2008); J. D. Le, Y. Pinto, N. C. Seeman, K. Musier-Forsyth, T. A. Taton, and R. A. Kiehl, Nano Lett. **4**, 2343 (2004).
[10] M. Maillard, L. Motte, A. T. Ngo, and M. P. Pileni, J. Phys. Chem. B **104**, 11871 (2000).
[11] M. Gonuguntla and A. Sharma, Langmuir **20**, 3456 (2004).
[12] J. N. O'Shea, M. A. Philips, M. D. R. Taylor, P. Moriarty, M. Brust, and V. R. Dhanak, Appl. Phys. Lett. **81**, 5039 (2002).
[13] G. Reiter, Phys. Rev. Lett. **68**, 75 (1992); Langmuir **9**, 1344 (1993); A. Sharma and G. Reiter, J. Colloid Interface Sci. **178**, 383 (1996); A. Sharma and R. Khanna, Phys. Rev. Lett. **81**, 3463 (1998); A. Sharma, Langmuir **14**, 4915 (1998); A. S. Padmakar, K. Kargupta, and A. Sharma, J. Chem. Phys. **110**, 1735 (1999); U. Thiele, M. Mertig, and W. Pompe, Phys. Rev. Lett. **80**, 2869 (1998); R. V. Craster and O. K. Matar, Rev. Mod. Phys. **81**, 1131 (2009).
[14] E. Pauliac-Vaujour and P. Moriarty, J. Phys. Chem. C **111**, 16255 (2007).
[15] C. P. Martin, M. O. Blunt, E. Pauliac-Vaujour, A. Stannard, P. Moriarty, I. Vancea, and U. Thiele, Phys. Rev. Lett. **99**, 116103 (2007).
[16] M. O. Blunt, C. P. Martin, M. Ahola-Tuomi, E. Pauliac-Vaujour, P. Sharp, P. Nativo, M. Brust, and P. J. Moriarty, Nat. Nanotechnol. **2**, 167 (2007).
[17] A. Stannard, C. P. Martin, E. Pauliac-Vaujour, P. Moriarty, U. Thiele, J. Phys. Chem. C **112**, 15195 (2008).
[18] E. Rabani, D. R. Reichman, P. L. Geissler, and L. E. Brus, Nature (London) **426**, 271 (2003).
[19] P. Siepmann, C. P. Martin, I. Vancea, P. J. Moriarty, and N. Krasnogor, Nano Lett. **7**, 1985 (2007).
[20] D. A. Weitz and M. Oliveria, Phys. Rev. Lett. **52**, 1433 (1984).
[21] R. Seshadri, G. N. Subbanna, V. Vijayakrishnan, G. U. Kulkarni, G. Ananthakrishna, and C. N. R. Rao, J. Phys. Chem. **99**, 5639 (1995).
[22] J. J. Benkoski, R. L. Jones, J. F. Douglas, and A. Karim, Langmuir **23**, 3530 (2007).
[23] P. Moriarty, M. D. R. Taylor, and M. Brust, Phys. Rev. Lett. **89**, 248303 (2002).
[24] C. P. Martin, M. O. Blunt, and P. Moriarty, Nano Lett. **4**, 2389 (2004).
[25] M. Elbaum and S. G. Lipson, Phys. Rev. Lett. **72**, 3562 (1994); S. G. Lipson, Phys. Scr., T **67**, 63 (1996); N. Samid-Merzel, S. G. Lipson, and D. S. Tannhauser, Phys. Rev. E **57**, 2906 (1998).
[26] M. Brust, M. Walker, D. Bethell, D. J. Schiffrin, and R. Whyman, J. Chem. Soc., Chem. Commun. **1994**, 801.
[27] J. Hu, X.-D. Xiao, D. F. Ogletree, and M. Salmeron, Surf. Sci. **344**, 221 (1995).
[28] L. Xu, A. Lio, J. Hu, D. F. Ogletree, and M. Salmeron, J. Phys. Chem. B **102**, 540 (1998).
[29] P. B. Miranda, L. Xu, Y. R. Shen, and M. Salmeron, Phys. Rev. Lett. **81**, 5876 (1998).
[30] See supplementary material at http://dx.doi.org/10.1063/1.3484941 for TEM, UV data, and a plot of the nanoparticles with aggregate size.
[31] K. J. Mutch, V. Koutsos, and P. J. Camp, Langmuir **22**, 5611 (2006).
[32] D. Weaire and N. Rivier, Contemp. Phys. **25**, 59 (1984).
[33] J. M. Gómez-Rodríguez, A. M. Baró, and R. C. Salvareeza, J. Vac. Sci. Technol. B **9**, 495 (1991).
[34] F. Zhao and J. Xu, Colloid Polym. Sci. **285**, 113 (2006).
[35] D. A. Weitz, J. S. Huang, M. Y. Lin, and J. Sung, Phys. Rev. Lett. **54**, 1416 (1985).